Preliminary Analysis of M and L Dwarf Surface Gravities in the NIRSPEC Brown Dwarf Spectroscopic Survey

Emily C. Martin[1], Gregory N. Mace[1], Ian S. McLean[1], Sarah E. Logsdon[1], Emily L. Rice[2,3]

[1] *University of California, Los Angeles, 475 Portola Plaza, Los Angeles, CA 90095*

[2] *Department of Engineering Science & Physics, College of Staten Island, City University of New York, 2800 Victory Blvd, Staten Island, NY 10314*

[3] *Department of Astrophysics, American Museum of Natural History, Central Park West at 79th Street, New York, NY 10024-5192*
[1]

Abstract.

Using previously published gravity-sensitive indices, we report on the analysis of near-infrared spectra for $\sim$ 80 M and L dwarfs. The spectra were obtained as part of the Brown Dwarf Spectroscopic Survey (BDSS) using NIRSPEC at the Keck Observatory, and each has a resolving power of R $\sim$ 2000 in the J band. With established gravity indices in the J band we can disentangle the degeneracy between temperature and age for brown dwarfs of various masses. By comparing a subset of the BDSS database with gravity indices defined at lower spectral resolution, we demonstrate that these indices also work well for higher resolution spectra. We then apply these techniques to M and L dwarfs in the BDSS to classify the diverse surface gravities of this large sample in a consistent manner. This analysis provides new age estimates for many M and L dwarfs, which will guide future studies of the young and old brown dwarf populations.

[1] emartin@astro.ucla.edu

1. Introduction

Since their discovery in the mid 1990's, the number of known brown dwarfs has increased dramatically. In large part, these discoveries were made using wide-field surveys such as 2MASS (Skrutskie et al. 2006), SDSS (York et al. 2000), UKIDSS (Lawrence et al. 2007), and WISE (Wright et al. 2010). The peak flux of a brown dwarf falls in the 1-5 μm range, so the advent of infrared arrays has allowed for many discoveries over the past 20 years. In addition to photometric surveys, spectroscopic follow-up has been the key to understanding the physical properties of brown dwarfs.

As summarized in Kirkpatrick (2005), in the red part of the optical regime and into the near infrared (NIR), brown dwarf spectra are dominated by spectral absorption features. Molecular bands of FeH, CO, and H_2O are common features of M and L dwarfs, as well as neutral atomic absorption lines from metals such as Na, K, Fe, Al, and Ca, and broad, continuum-like H_2 collision-induced absorption. The varying strengths (and presence) of different lines determines spectral type and provides insight into other physical properties, such as surface gravity and metallicity.

1.1 Brown Dwarf Spectroscopic Survey

In 1999, the Near-Infrared Spectrometer (NIRSPEC; McLean et al. (1998)) was commissioned for the W.M. Keck II 10m telescope on Mauna Kea in Hawaii. This instrument was designed for both moderate (R=$\lambda/\Delta\lambda \sim$ 2000) and high (R$\sim$20,000) resolution spectroscopy in the 1-5 μm wavelength regime, making it ideally suited to the study of brown dwarfs. For this reason, Ian McLean and collaborators chose NIRSPEC to take spectra of a large sample of brown dwarfs and low-mass stars, known as the Brown Dwarf Spectroscopic Survey (BDSS). The primary goal of the BDSS as outlined in McLean et al. (2003) is to gather a large database of NIR spectra of low-mass stars and brown dwarfs in order to examine their spectral properties and make comparisons to evolutionary and atmospheric models. In McLean et al. (2003), the first set of moderate resolution data are presented, and these are followed by high resolution spectra in McLean et al. (2007) and Rice et al. (2010). Over the past 15 years, the BDSS team at the University of California, Los Angeles has accumulated many infrared spectra of brown dwarfs and low-mass stars (see §2).

1.2 Surface Gravity as an Age Indicator

Formation and evolution theory of brown dwarfs suggests that M and L dwarfs are a mixture of very low-mass stars and high-mass brown dwarfs, while T and Y dwarfs are entirely substellar (Burrows et al. 2001; Cushing et al. 2011). Degeneracy between mass, temperature, and age makes it difficult to accurately characterize a brown dwarf solely on its spectral type. For example, a spectral type L-dwarf could conceivably be a very old low-mass star, a moderate-aged more massive brown dwarf, or a newly formed low-mass brown dwarf. A brown dwarf's surface gravity ($g = GM/R^2$) will increase as it ages and its radius shrinks. Luckily, brown dwarfs have several spectral features which can indicate the strength of surface gravity, thus allowing us to disentangle mass and age.

In particular, the strength and equivalent widths (EW) of FeH, Na I, and K I lines in optical (Cruz et al. 2009) and NIR spectra (McLean et al. 2003; McGovern et al. 2004; Allers & Liu 2013) are shown to be correlated to surface gravity. For dwarfs with lower surface gravities, the atmospheric pressure is lower so alkali metals tend to be more ionized. Thus, they have weaker neutral alkali metal absorption lines. For higher surface gravities, higher atmospheric pressure allows for more recombination to occur and thus larger amounts of neutral potassium and sodium are available as absorbers. By studying how the strengths of these lines vary with spectral type and gravity, we can estimate ages of brown dwarfs from their NIR spectra.

Allers & Liu (2013) (hereafter A13) presents a NIR gravity classification system based on moderate (R$\sim$750) and low (R$\sim$100) resolution spectra of a large sample of brown dwarfs. The A13 gravity classification scheme is determined primarily on the strength of several Na, K, and

FeH lines in the NIR. In this paper, we compare the A13 gravity classifications to an overlapping sample from the BDSS using medium resolution (R∼2150) spectra. We then apply the A13 gravity classification technique to a large sample of BDSS targets. In §2 we present our sample and in §3 we describe the calculation of potassium line equivalent widths as a diagnostic for surface gravity. In §4, we present the FeH$_J$ index, and in §5 we describe our future plans to determine gravity classifications for the entire set of M and L dwarfs in the BDSS, as well as plans to extend the gravity classification scheme for T dwarfs.

2. Sample

For this preliminary analysis, we examine spectra from the BDSS observed between 2000 and 2009. In total, there are ∼ 80 low-mass stars and brown dwarfs with spectra in the N3 filter (J band) at a resolution of R ∼ 2150 observed using the moderate-resolution, non-echelle mode on NIRSPEC. Our sample covers a range of spectral types from M5 to L8, with 16 of our targets overlapping the sample presented in A13.

2.1 Observations

Targets were observed using the strategy described in McLean et al. (2003). Typically, 300 s exposures were taken in nod pairs of 20" separation along the 42" slit. Fainter objects were observed for longer, as needed. For the medium resolution mode, the slit is 0.38" wide (two pixels). These nods were generally done in ABBA format for a total observing time of 20 minutes per target. A0V stars at similar airmass were chosen for each target to calibrate the spectra. If there were no nearby A0V stars, calibrators of spectral type B9-A3 were used instead. In N3, the A0V stars typically only contain the Paβ absorption line at 1.282 μm , which is easily removed from the spectrum by interpolation. In addition to calibrators, flat field and dark frames were taken, as well as spectra of Ne and Ar lamps for wavelength calibration.

2.2 Data Reduction

Data reduction was performed by various collaborators in the BDSS team using the REDSPEC software designed specifically for NIRSPEC data as outlined in McLean et al. (2003) and Rice et al. (2010). The code first corrects for spatial and spectral distortion on the array using the Ne and Ar lamp lines with wavelengths taken from NIST (http://physics.nist.gov). The nod pairs are then background subtracted and divided by the flat field. OH emission lines and bad pixels are removed as well. Spectra are obtained by summing over a range of ∼10 pixels (depending on seeing) and then dividing by the calibrator spectrum to remove telluric features. Each pair of spectra was normalized and combined with other pairs (when available) to achieve higher signal-to-noise ratio (SNR). This sample contains targets with SNR ∼10-200, although the majority of the spectra have SNR of at least 20, as required by the BDSS. Finally, heliocentric velocity corrections were applied to the normalized spectra.

3. Equivalent Widths

We compute equivalent widths (EW) for the four potassium lines in the J band. For accurate comparison, we use the same line and continuum windows as defined in A13 and as shown in Figure 1. The blue, green, and red regions indicate the line windows used, while the grey shows the continuum windows. The KI doublet at 1.1692 μm and 1.1778 μm share the continuum windows

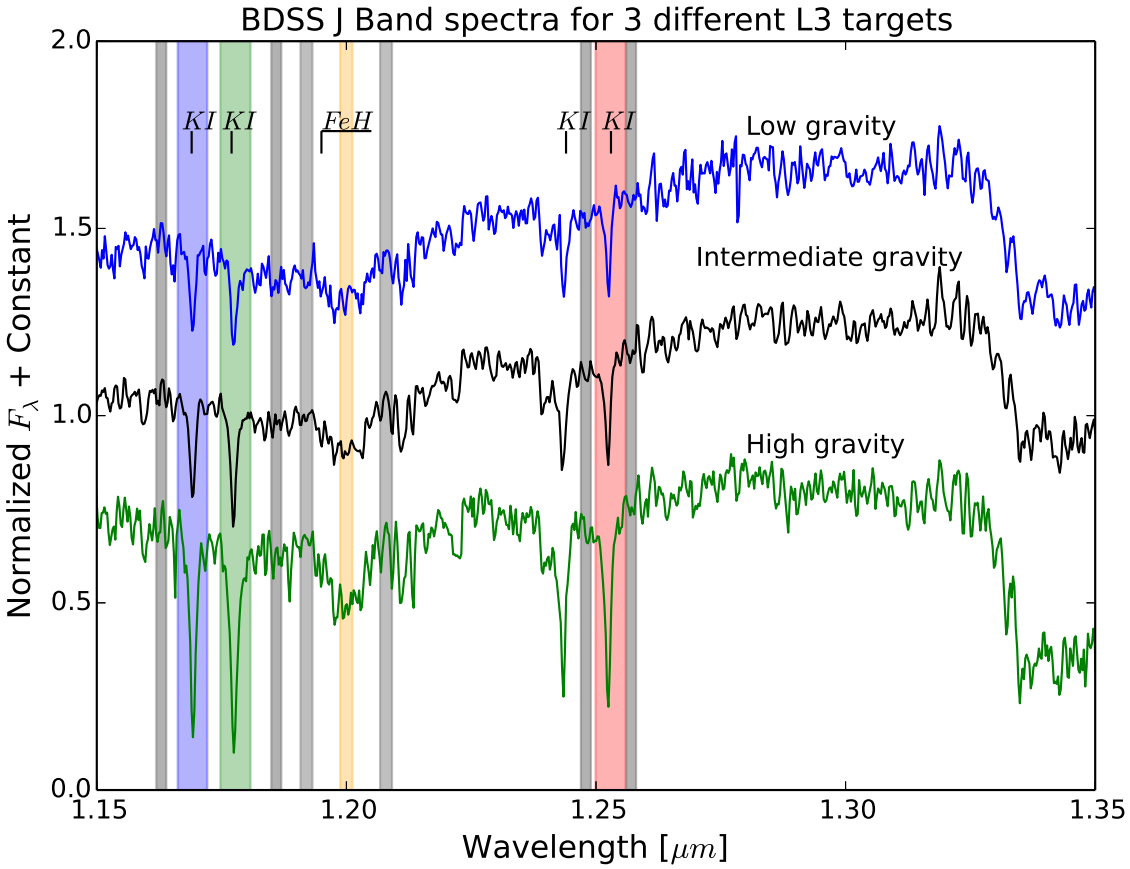

Figure .1: Location of Equivalent Width and FeH$_J$ windows as defined by A13, shown for NIRSPEC spectra of native resolution, R∼2150 for three different L3 targets. The colored regions indicate the line windows used, while the grey shows the continuum windows. The doublet at 1.1692 μm and 1.1778 μm share the continuum windows on either side of the doublet, and the 1.2437 μm and 1.2529 μm lines share the continua surrounding the 1.2529 μm line. A13 excluded the 1.2437 μm line because of the FeH contamination on the blue side of the line. For this paper, all calculations were performed on the native resolution (R∼2150); A13 calculated EWs using R∼750.

on either side of the doublet, and the 1.2437 μm and 1.2529 μm lines share the continua surrounding the 1.2529 μm line. A13 chooses to exclude the 1.2437 μm line because of the FeH contamination on the blue side of the line.

Using a procedure similar to A13, we estimate a continuum using a linear regression fit to the flux in the continuum windows. The EW calculations are performed using a Monte Carlo (MC) technique of 1000 iterations. For each iteration, the flux in each pixel is multiplied by a random number drawn from a Gaussian centered at 1 with a sigma determined by the SNR of that pixel. The equivalent width for each flux modulation is recorded, and we then compute the median and standard deviation of the EWs as the best estimate and 1σ uncertainties.

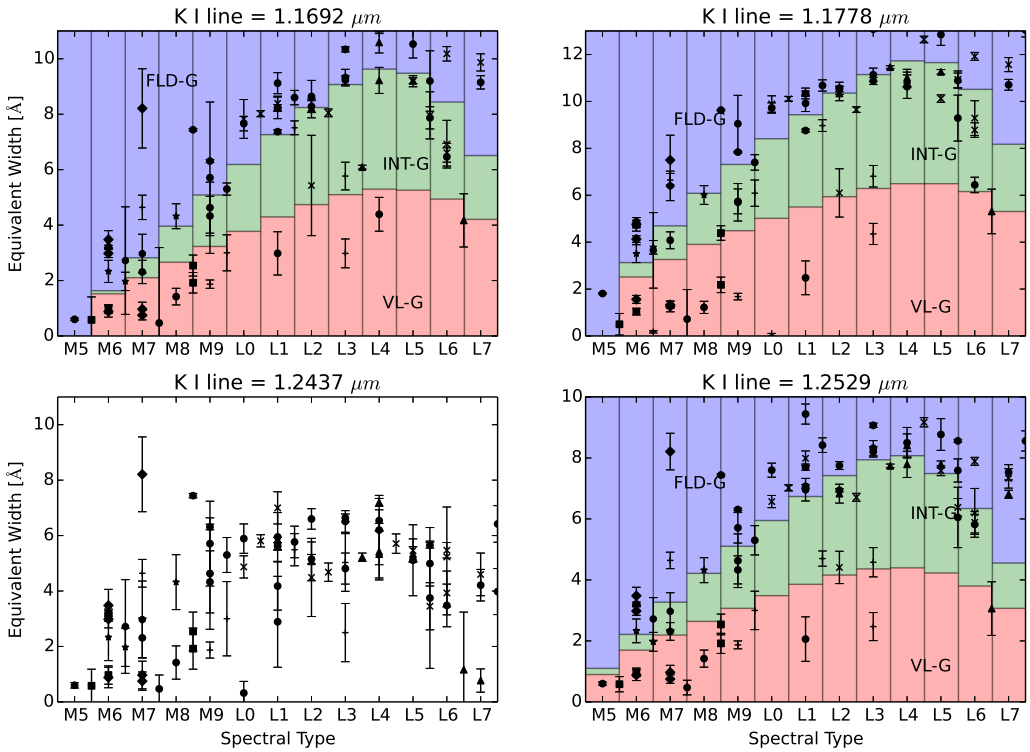

Figure .2: K I equivalent width versus spectral type for BDSS targets. For the three K I lines used by A13, regions are shaded to denote the locations of cutoffs for various gravity designations. For each line, targets lying within the salmon-pink shaded region receive a score of "2", targets within the green shaded region receive a score of "1" and targets within the purple shaded region receive a score of "0". The three values for each target are then averaged to determine a final gravity classification, where VL-G is very low gravity, INT-G is intermediate gravity, and FLD-G is "field", or high, gravity. For the 1.2437 μm line, A13 does not define values due to contamination of the line by FeH absorption. Various symbols represent different populations of stars: '+' is a known young object, 'x' is in a binary system, squares are in Rho Ophiuci, octagons are in the Pleiades, diamonds are in Upper Scorpius, triangles have peculiar spectra (generally red or blue), and 'o' is the default.

In Figure 2, we show results for the four K I Equivalent Widths versus NIR spectral type, calculated using the Monte Carlo technique. Shaded regions in Figure 2 show the boundaries proposed by A13 to designate low, intermediate, and high surface gravity objects. Objects lying within the salmon shaded regions receive a score of "2" (indicating low gravity), objects in the green shaded regions receive a score of "1" (intermediate gravity), and objects within the purple shaded regions receive a score of "0" ("field" or high gravity). The scores are then averaged for each object to obtain a gravity classification.

3.1 Comparison to Allers & Liu (2013)

A13 proposes a quantitative system for determining surface gravities and age estimates for $\sim$ 70 M and L dwarfs. They first chose known gravity-sensitive features in the NIR spectra of M and L dwarfs, and then created indices that distinguished known young ($\leq$ 10 Myr) dwarfs from known older (field, $>$ 300 Myr) dwarfs. A13 introduces three designations for surface gravity to be used in conjunction with spectral type to characterize brown dwarfs. The designation "FLD-G" is given to older dwarfs, with gravity indices similar to those of typical field dwarfs. "INT-G" designates objects of intermediate gravity. These objects lie approximately in between the young and old populations. Finally, "VL-G" objects have spectral indices consistent with objects exhibiting signs of very low gravity.

In Figure 3, our EW results are plotted against the results from A13. We have 12 overlapping targets with the A13 moderate resolution SpeX sample. Due to higher resolution and good signal-to-noise using NIRSPEC, our estimated uncertainties tend to be smaller than in A13. However, a few of the targets have a SNR of $\sim$10, which tends to produce much larger uncertainties on the estimated EW values.

With only two exceptions, our values match well with those of A13. There is considerably more scatter for the targets with lower equivalent width values, but these do not appear to be systematically skewed. The two noticeable exceptions in Figure 3 are G196-3B and 2MASS 0141-4633. The outliers are probably a systematic effect due to lower SNR observations, as indicated by the larger error bars. 2MASS 0141 is only an outlier for one out of three K I EW values; the other two K I EW measurements are consistent with A13. In the case of G196-3B, it is most likely that scattered light from the brighter primary affected the observations.

4. FeH$_J$ Index

In addition to the KI equivalent width measurements, we also studied the FeH$_J$ index as defined by A13 for moderate (R$\sim$750-2000) data. The FeH$_J$ index is based on the 1.2 μm FeH absorption feature. In Figure 1, the window used for computing the index is marked in yellow, and the windows used for estimating the continuum are shown in grey.

As was done for the EW calculations, we ran a Monte Carlo process to modulate the flux in each pixel by a random number drawn from a Gaussian, with a width defined by the SNR. Next, we compute the index for 1000 iterations, and used the median and standard deviation as our best estimate and one-sigma uncertainties. In addition to using the native resolution (R $\sim$ 2150), we also convolved our spectra with Gaussians to smooth them out and mimic lower resolution data at R=750. This Gaussian smoothing was done using the astropy[2] convolution via 1D Gaussian kernel after each iteration of flux modulation, before calculating the index values. Our results are shown in Figure 4.

Shaded regions denote cutoffs for gravity index scores in a similar manner to Figure 2. In Figure 5, we compare our results to those of A13. Our results agree quite well, with the exception of one outlier, G196-3B. Again, we suspect that scattered light from the primary could be the cause of this particular outlier.

[2]http://www.astropy.org

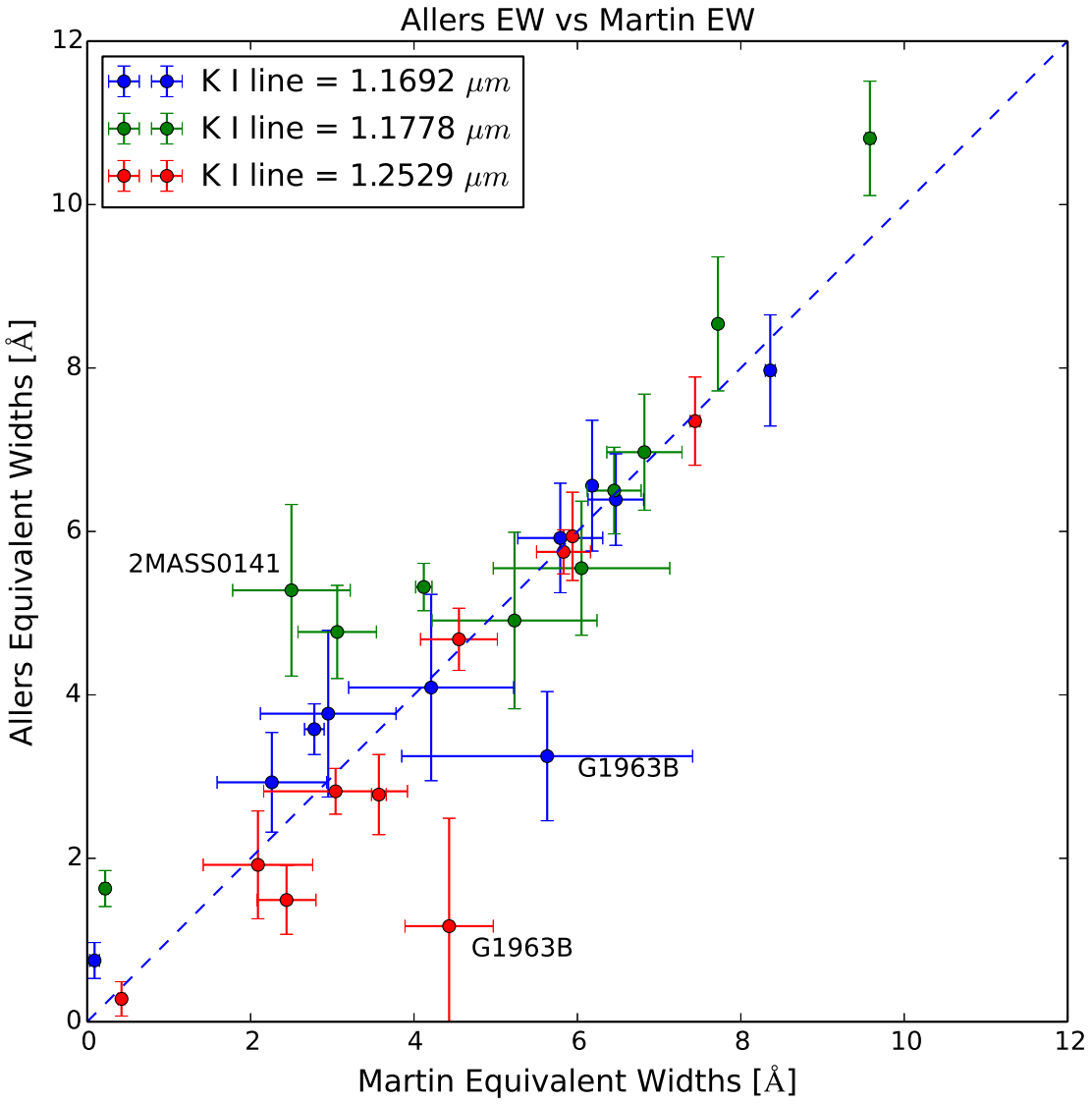

Figure .3: Comparison between A13 and Martin et al. calculated equivalent widths for 3 of the K I lines. In general, the error bars presented in this paper are smaller because of the higher resolution of NIRSPEC data. However, a few objects have data with SNR$\sim$10, which causes much larger uncertainties in the EW measurements. The 2 σ outliers are noted above.

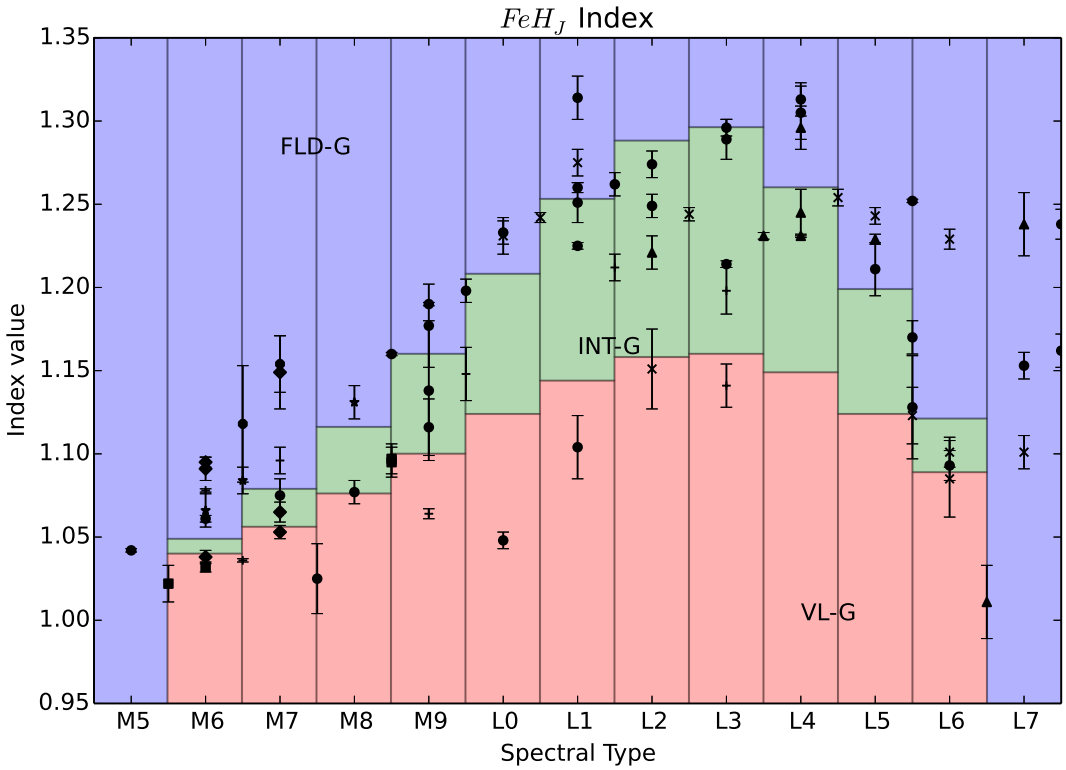

Figure .4: Low and Moderate Resolution gravity index values for R$\sim$ 2150 spectra. Shaded regions denote cutoffs for gravity index scores, as described in Figure 2. A13 did not define gravity-type cutoffs for objects M5 and earlier or L7 and later. Objects lying within the salmon-pink shaded regions receive a score of "2" (indicating low gravity), objects in the green shaded regions receive a score of "1" (intermediate gravity), and objects within the purple shaded regions receive a score of "0" ("field" or high gravity). The scores are then averaged for each object to obtain a gravity classification.

5. Future Work

The BDSS has grown significantly over the past 15 years. Our team has amassed over 300 spectra of M, L, and T dwarfs. We plan to continue the surface gravity analysis presented in this paper by extending it to the entire sample of M5-M9 dwarfs and all L dwarfs. Such a large sample should enable a better statistical analysis of the distinction between high and low surface gravity objects. We hope to develop designations for the low and intermediate gravity objects by fitting lines to our EW vs spectral type data. We also plan to extend the analysis for T dwarfs, and define useful indices to determine surface gravities of later type dwarfs.

6. Conclusions

Using a sample of $\sim$ 80 M- and L-type dwarfs with R$\sim$2150 resolution spectra from NIRSPEC on Keck, we calculate equivalent widths of potassium lines and determine other gravity indices as proposed by A13. By comparison to an overlapping sample of 16 targets with the A13 sample, we find that our measurements and gravity scores are consistent with A13. In general, our gravity indices have smaller uncertainties than A13 due to higher resolution and higher signal-to-noise data. We use a Monte Carlo method of 1000 iterations, and we propagate uncertainties in flux based on the S/N of the target spectrum. We then apply the A13 technique to a large sample of BDSS J band observations of low mass stars and brown dwarfs to determine their gravity types.

Acknowledgements. The data presented herein were obtained at the W.M. Keck Observatory, which is operated as a scientific partnership among the California Institute of Technology, the University of California and the National Aeronautics and Space Administration. The Observatory was made possible by the generous financial support of the W.M. Keck Foundation. The authors wish to recognize and acknowledge the very significant cultural role and reverence that the summit of Mauna Kea has always had within the indigenous Hawaiian community. We are most fortunate to have the opportunity to conduct observations from this mountain. This research made use of Astropy, a community-developed core Python package for Astronomy Astropy Collaboration et al. (2013)

References

Allers, K. N., & Liu, M. C. 2013, ApJ, 772, 79

Astropy Collaboration, Robitaille, T. P., Tollerud, E. J., et al. 2013, A&A, 558, A33

Burrows, A., Hubbard, W. B., Lunine, J. I., & Liebert, J. 2001, Reviews of Modern Physics, 73, 719

Cruz, K. L., Kirkpatrick, J. D., & Burgasser, A. J. 2009, AJ, 137, 3345

Cushing, M. C., Kirkpatrick, J. D., Gelino, C. R., et al. 2011, ApJ, 743, 50

Kirkpatrick, J. D. 2005, ARA&A, 43, 195

Lawrence, A., Warren, S. J., Almaini, O., et al. 2007, MNRAS, 379, 1599

McGovern, M. R., Kirkpatrick, J. D., McLean, I. S., et al. 2004, ApJ, 600, 1020

McLean, I. S., Becklin, E. E., Bendiksen, O., et al. 1998, Proc. SPIE, 3354, 566

McLean, I. S., McGovern, M. R., Burgasser, A. J., et al. 2003, ApJ, 596, 561

McLean, I. S., Prato, L., McGovern, M. R., et al. 2007, ApJ, 658, 1217

Rice, E. L., Barman, T., Mclean, I. S., Prato, L., & Kirkpatrick, J. D. 2010, ApJS, 186, 63

Skrutskie, M. F., Cutri, R. M., Stiening, R., et al. 2006, AJ, 131, 1163

Wright, E. L., Eisenhardt, P. R. M., Mainzer, A. K., et al. 2010, AJ, 140, 1868

York, D. G., Adelman, J., Anderson, J. E., Jr., et al. 2000, AJ, 120, 1579

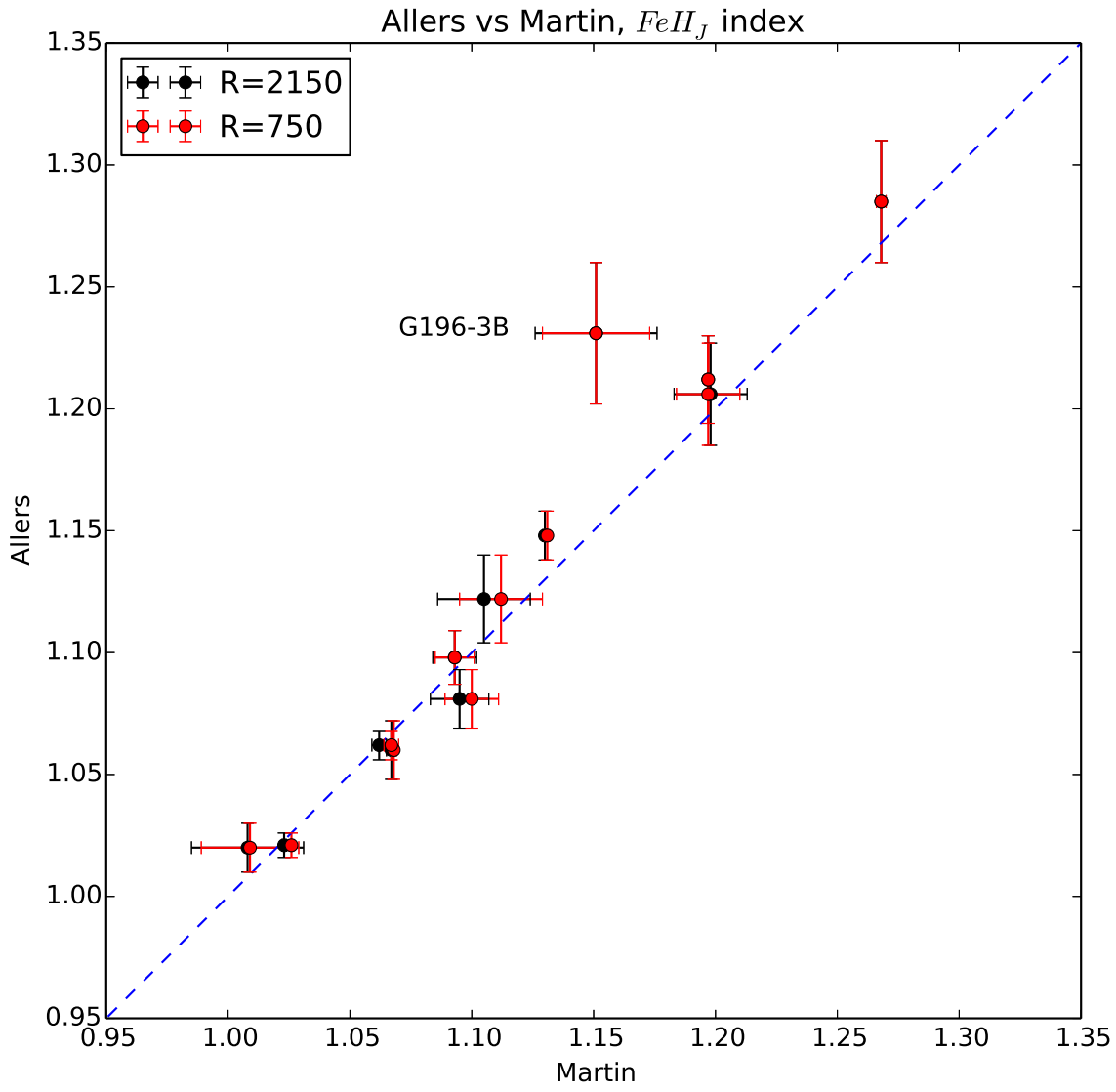

Figure .5: Comparison between A13 and Martin et al. calculated FeH$_J$ index values. Native BDSS resolution of R∼2150 as well as the convolved R∼750 index values are plotted. Both resolutions agree completely within the uncertainties. Therefore, using R∼2150 spectra to calculate the FeH$_J$ index is a valid replacement for R∼750 spectra.